The solution of Eq. (6) for a given ml/M is denoted as k_D. Table 1 presents values of k_D for given ml/M, and Fig. 1 plots $\sigma(0)/\sigma(0)_{cl}$ for a wide range of k.

Rotating Disk

The appropriate equations are

$$\rho\Omega^2(r + u) + d\sigma_r/dr + (\sigma_r - \sigma_\theta)/r = 0 \quad (7)$$

$$\epsilon_r = du/dr = (\sigma_r - \nu\sigma_\theta)/E \quad (8)$$

$$\epsilon_\theta = u/r = (\sigma_\theta - \nu\sigma_r)/E \quad (9)$$

Inverting Eqs. (8) and (9) and substituting the results into Eq. (7) yields the displacement equilibrium equation

$$r^2d^2u/dr^2 + rdu/dr + [\Omega_*{}^2(r/b)^2 - 1]u = \Omega_*{}^2r^3/b^2 \quad (10)$$

where

$$\Omega_*{}^2 = (1 - \nu^2)\rho\Omega^2b^2/E \quad (11)$$

The general solution for u, σ_r, and σ_θ are then given by

$$u/b = AJ_1(\Omega_*r/b) + BY_1(\Omega_*r/b) - (r/b) \quad (12)$$

$$(1 - \nu^2)\sigma_r/E = A[\Omega_*J_0(\Omega_*r/b) - (b/r)(1 - \nu)J_1(\Omega_*r/b)] + B[\Omega_*Y_0(\Omega_*r/b) - (b/r)(1 - \nu)Y_1(\Omega_*r/b)] - (1 + \nu) \quad (13)$$

$$(1 - \nu^2)\sigma_\theta/E = A[(b/r)(1 - \nu)J_1(\Omega_*r/b) + \nu\Omega_*J_0(\Omega_*r/b)] + B[(b/r)(1 - \nu)Y_1(\Omega_*r/b) + \nu\Omega_*Y_0(\Omega_*r/b)] - (1 + \nu) \quad (14)$$

Applying the boundary conditions $u(a) = \sigma_r(b) = 0$ yields for A and B,

$$A = [(1 + \nu)Y_1(\Omega_*a/b) - (a/b)\Omega_*Y_0(\Omega_*) + (a/b)(1 - \nu)Y_1(\Omega_*)]/C \quad (15)$$

$$B = [(a/b)\Omega^*J_0(\Omega^*) - (a/b)(1 - \nu)J_1(\Omega^*) - (1 + \nu)J_1(\Omega_*a/b)]/C \quad (16)$$

where

$$C = Y_1(\Omega_*a/b)[\Omega_*J_0(\Omega_*) - (1 - \nu)J_1(\Omega_*)] + J_1(\Omega_*a/b)[(1 - \nu)Y_1(\Omega_*) - \Omega_*Y_0(\Omega_*)] \quad (17)$$

The Ω_* at which the instability occurs is given by $C = 0$ and is denoted by Ω_{*D}. These values are given in Table 2 for $\nu = 0.3$ and various a/b ratios. The corresponding classical results are given by

$$(u/b)_{cl} = A_*r/b + B_*b/r - \Omega_*{}^2(r/b)^3/8 \quad (18)$$

$$(1 - \nu^2)(\sigma_r)_{cl}/E = A_*(1 + \nu) - B_*(b/r)^2(1 - \nu) - \Omega_*{}^2(r/b)^2(3 + \nu)/8 \quad (19)$$

$$(1 - \nu^2)(\sigma_\theta)_{cl}/E = A_*(1 + \nu) + B_*(b/r)^2(1 - \nu) - \Omega_*{}^2(r/b)^2(1 + 3\nu)/8 \quad (20)$$

and applying the boundary conditions $u_r(a)_{cl} = \sigma_r(b)_{cl} = 0$ yields

$$A_* = \Omega_*{}^2[(a/b)^4(1 - \nu) + (3 + \nu)]/8C_* \quad (21)$$

$$B_* = \Omega_*{}^2[(a/b)^4(1 + \nu) - (a/b)^2(3 + \nu)]/8C_* \quad (22)$$

Table 2 Ω_{*D} vs a/b for $\nu = 0.3$

$\nu = 0.3$	
a/b	Ω_{*D}
0.10	2.088
0.30	2.404
0.50	3.183
0.70	5.194
0.90	15.605

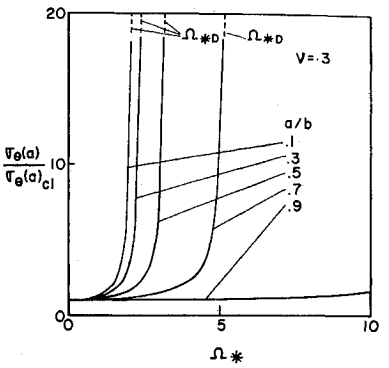

Fig. 2 Tangential hoop stress ratio $\sigma\theta(a)/\sigma\theta(a)_{cl}$ vs rotational parameter Ω^*.

where

$$C_* = (a/b)^2(1 - \nu) + (1 + \nu) \quad (23)$$

It is noted that no instability is present in the classical results.

Preliminary investigation showed that $\sigma_\theta(a)$ is still the largest stress (as it is in the classical case) so the important result is the ratio $\sigma_\theta(a)/\sigma_\theta(a)_{cl}$ plotted vs Ω_* for various a/b ratios. These results are shown in Fig. 2.

Discussion

The preceeding two problems have been analyzed assuming linear elastic behavior. It is to be noted that if the material used has a nonlinear softening behavior† the instability will still exist and in fact will occur at a much lower rotational speed.

† i.e. strain hardening material.

Streamwise Vortices in Reattaching High-Speed Flows: A Suggested Approach

JEAN J. GINOUX*
von Kármán Institute, Belgium

THERE is experimental evidence of the systematic development of streamwise vortices in reattaching two-dimensional supersonic flows. They have a remarkable periodicity with a wavelength equal to two to three times the

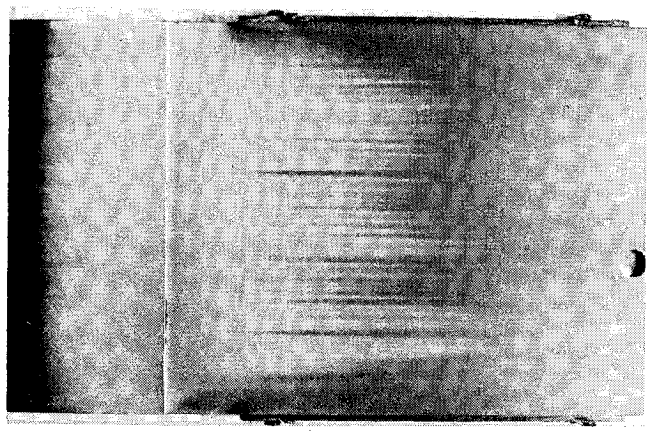

Fig. 1 Spanwise variation of skin friction for $M = 5.3$ flow over a backward facing step.

Received December 15, 1970.

* Professor at Brussels University and Head of the High Speed Laboratory at the von Kármán Institute.

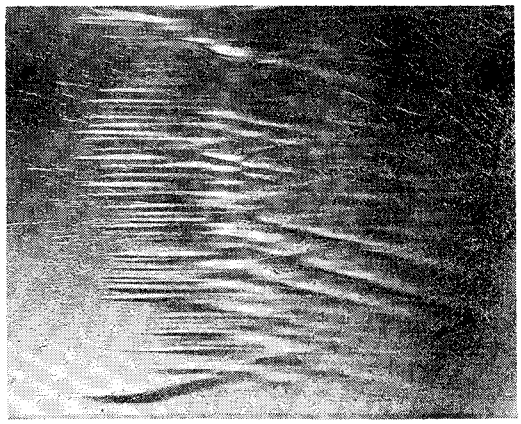

Fig. 2 Spanwise variation of heat transfer for $M = 5.3$ flow over a backward facing step.

boundary-layer thickness over a large range of Mach numbers.[1,2] They were observed in laminar, transitional and turbulent flows. One important practical effect of these vortices is to produce large spanwise variations of the heat transfer and skin friction with local peaks several times larger than the spanwise average value.[3] Examples are shown in Figs. 1 and 2 for a Mach number 5.3 flow over a two-dimensional backward facing step. The striation pattern in Fig. 1, obtained by a sublimation technique of surface flow visualization, demonstrates the spanwise variation of the skin friction. In Fig. 2, grooves scorched into natural wax in the reattachment flow region are indicative of the heat transfer variations. Also seen is the cross-hatched pattern which develops in the turbulent region of the flow. Figure 3 illustrates the skin-friction variations on an axisymmetric hollow cylinder flare model at the same freestream Mach number.

The author has shown that extremely weak initial disturbances existed in the two-dimensional boundary layer upstream of separation because of small imperfections in the leading edge thickness. These were obviously irregularly distributed in the spanwise direction, and the reason why an orderly pattern of pairs of intense counter-rotating vortices develop as the supersonic flow is approaching reattachment is not fully known yet, although an attempt has recently been made[4] to study the stability of a two dimensional stagnation flow at low speeds.

Oil flow visualizations in the reattachment region[1,5] for turbulent supersonic flow over backward facing steps tend to suggest that the flow does not reattach in the classical two-dimensional sense, i.e., on a transverse line along which the skin friction vanishes. It seems rather that flow attachment involves typical three-dimensional singularities (saddle and nodal points of attachment) periodically distributed along a straight line normal to the freestream direction. This is schematically illustrated in Fig. 4 which shows limiting streamlines in the reattachment region as suggested by oil flow visualizations. Nodal and saddles points of attachment are evenly distributed along the "attachment line" AB.

Therefore, although one can conceive that orderly arrays of pairs of counter-rotating vortices of the Görtler type, existing in the free shear layer as a result of streamline curvature, imply this type of flow attachment, one can also conceive that vortices are being developed as a result of this being the only possible type of attachment in the presence of any weak initial disturbance in the approaching boundary layer. It is believed that this approach is worth further investigation.

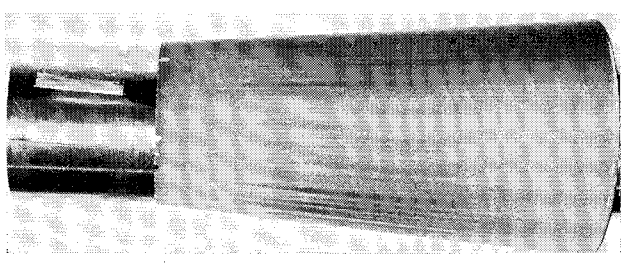

Fig. 3 Spanwise variation of skin friction for $M = 5.3$ flow over a hollow cylinder flare model.

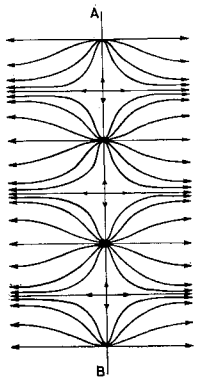

Fig. 4 Schematic configuration of the limiting streamlines in the reattachment region.

References

[1] Ginoux, J., "Experimental Evidence of Three Dimensional Perturbations in the Reattachment of a Two Dimensional Laminar Boundary Layer at M = 2.05," TN 1, 1958, von Kármán Institute, Belgium.

[2] Ginoux, J. "Effect of Mach Number on Streamwise Vortices in Laminar Reattaching Flow; TN 26, 1965, von Kármán Institute, Belgium.

[3] Ginoux, J., "Streamwise Vortices in Laminar Flow," AGARDograph 97, 1965.

[4] Kestin, J. and Wood, R. T., "On the Stability of Two Dimensional Stagnation Flow," *Journal of Fluid Mechanics*, Vol. 44, Pt. 3, 1970.

[5] Roshko, A. and Thomke, G., "Observations of Turbulent reattachment behind an Axisymmetric Downstream-Facing Step in Supersonic Flow," *AIAA Journal*, Vol. 4, No. 6, June 1966, pp. 975–980.

Inequality Constraints in Primer-Optimal, N-Impulse Solutions

D. J. Jezewski* and N. L. Faust†
NASA Manned Spacecraft Center, Houston, Texas

Introduction

THE primer vector approach to the solution of optimal N-impulse trajectory problems has not been extended to solutions in which the imposed constraints are not readily expressed in terms of the control variables. In primer vector solutions,[1–3] the cost is expressed as a sum of the applied impulsive velocity increments. The total differential of this cost is expressed in terms of the differentials of the control variables (that is, the positions and times of all intermediate impulses) and possibly in terms of some variable of the initial and final boundary conditions. Hence, equality constraints at the boundaries of the solution can be readily handled by at most a transformation of coordinates. Inequality constraints at the boundaries of the solution require more attention to the application of the constraints. When the inequality constraint is violated on the boundary, the procedure adopted is to place the control on the boundary and to set the gradient of the cost function with respect to this control to zero. This

Received July 17, 1970; revision received December 30, 1970.

* Aerospace Engineer, Mission Planning and Analysis Division. Member AIAA.

† Aerospace Engineer. Associate Member AIAA.